JOURNAL OF MATERIALS SCIENCE 28 (1993) 5630–5636

High-temperature deformation of solution-treated Al–0.6% Si-1% Mn–0.7 Fe alloy

A. M. HAMMAD, Z. M. YOUSEF, A. EL-NAKOOH
Nuclear Metallurgy Department, Nuclear Research Centre, Atomic Energy Establishment, P.O.B. 13759, Cairo, Egypt

The tensile properties of Al–0.6% Si–1% Mn–0.7% Fe alloy were investigated in the temperature range 295–773 K, to assess the effect of the precipitation of Si, Mn and Fe during ageing and deformation on the mechanical properties. The alloy showed a pronounced drop in ductility at elevated temperatures. Elongation-to-fracture versus temperature-of-deformation curves are evaluated as a function of the strain rate. The elevated-temperature yield and ultimate tensile strength (UTS), ductility, strain-rate sensitivity and strain-hardening exponent have a strain-rate dependence. The minimum in the strain-rate sensitivity versus temperature curve is coincident with the elongation minimum temperature. At low and high temperature ranges the flow could be represented by the constitutive equations $\sigma = K_2 \varepsilon^n$ and $\sigma = K_3 \dot{\varepsilon}^m$, respectively. There is also a discussion of the activation energy for deformation in the vicinity of the ductility minima and from plotting the logarithm of the strain rate versus the reciprocal absolute temperature at a constant yield strength (18 MN m^{-2}). A tentative model based on the diffusion of Si, Fe and Mn in Al and the subsequent precipitation of Si, $FeAl_3$, $MnAl_6$ and α–$Al_{12}Mn_3Si$ is postulated to explain the loss in ductility at high temperatures and the corresponding change in strength. An attempt is made to correlate strength, ductility and structural changes at elevated temperatures.

1. Introduction

Although in many practical situations materials are subjected to both high temperatures and mechanical properties, most of the precipitation experiments reported to date deal only with the effect of the former. To be successful, materials engineers must have a good understanding of the relationship between structure and properties. Several commercially important aluminium-alloy systems have been subjected to careful investigation of the structures existing at various stages of the precipitation process. So research and development are important in the field of aluminium alloys, particularly for high-strength, age-hardening alloys. The basic requirement for an alloy to acquire high strength through heat treatment is that it should undergo a phase transformation or structural changes in the solid state. The precipitation reaction is the most widely investigated in this connection. A large number of commercial alloys, particularly based on aluminium are capable of hardening via precipitation. In particular, the improved strength of Al alloys containing one or more alloying elements like Cu, Mg, Zn, Fe, Mn and Si is attributed to precipitation hardening. Si is, after Fe, the highest level impurity in commercial Al. The commercial importance of Al–Si alloys is based on their high fluidity and low shrinkage in casting, brazing and welding applications as well as their high corrosion resistance. Mn is a common impurity in primary Al. It increases its strength either in solid solution or as a finely precipitated intermetallic phase. As an addition, it is used to increase strength and to control the grain structure. As a dispersed precipitate, it is effective in slowing recovery and in preventing grain growth. Moreover, the increase in the strength of the alloy depends on the structure, spacing, size, shape and distribution of the precipitated particles, as well as on the degree of structural and crystallographic coherency with the matrix. Thus, studies concerning structure–property correlations and the development of methods of improving the strength of the materials without a significant loss of ductility constitute relevant research which is of technological significance. The two most important test parameters affecting tensile properties are the test temperature and the strain rate. The variation in strength and ductility with test temperatures have been studied for commercial grades of aluminium [1, 2], Al–Ge[3], Al–Si and Al–Fe [4], Al–Mg [5–9], Al–Zn [10], Al–Cu [11] and for other alloys [12–15] and have been correlated separately with the structural changes.

This work presents the effect of Si, Mn and Fe on the 0.2% yield strength, ultimate tensile strength (UTS), work hardening and ductility of solution treated Al–0.6% Si–1% Mn–0.7% Fe alloy in the temperature range 295–773 K. The variations in properties have been correlated with the structural changes accompanying the deformation.

0022–2461

2. Experimental procedure

The starting material was in the form of sheets with the chemical composition given in Table I.

Tensile specimens having a gauge length of 15 mm and a width of 3 mm were die stamped from 1 mm thick strips. As surface conditions strongly influence the mechanical properties, only specimens without surface flaws were accepted for the tensile tests. Tensile specimens were solution treated at 803 K for 1 h, followed by water quenching. The grain size, as measured by the linear-intercept method, 240 μm.

Tensile tests were performed in the temperature range 295–773 K on an Instron Universal Testing Machine at strain rates of 5.56×10^{-5}, 5.56×10^{-4} and $5.56\times10^{-3}\ s^{-1}$. The instrument was equipped with a tubular furnace which could be located around the tensile specimen and the temperature could be maintained to $\pm$ 2 K. At a given temperature the specimen was homogenized for 10 min before commencing deformation. Reproducibility of the results was ensured by performing two tests on average for each combination of temperature and strain rate.

3. Results

The variation with test temperature of the elongation-to-fracture, 0.2% yield strength and UTS of solution-treated Al–0.6% Si–1% Mn–0.7% Fe alloy, tensile tested at three strain rates is shown in Figs 1, 3 and 4, respectively. To establish that the extrema observed were genuine, for each condition, two or more tests were performed. The average ductility was reported as the elongation-to-fracture. The results indicate that there are two peaks and two ductility drops. The temperature at which the drop in ductility starts, and/or the minimum ductility occurs, is strain-rate dependent and decreases with decreasing strain rate. The values of ductility at these temperatures were also found to decrease when the strain rate decreased.

The ductility dependence on the strain rate of specimens at different test temperatures indicates that the phenomenon responsible for the loss in ductility is diffusion controlled [1, 3, 6, 10–15]. To understand the diffusion mechanism and the diffusing species the shift in temperature should be correlated with strain rate using the Arrhenius equation, $\dot{\varepsilon} = A \exp(-Q/RT)$. Where, $\dot{\varepsilon}$ is the strain rate, A is a constant, R is the gas constant, T is the test temperature (in K) and Q is the activation energy.

Accordingly, the dependence of the ductility of the alloy on the strain rate at different test temperatures, and the mechanism relating these variables, can be represented by plotting the logarithm of the strain rate against the reciprocal of absolute temperature corresponding to the minimum ductility (Fig. 2). The relationship is linear with an activation energy of 93.3 kJ mol^{-1} (22.1 kCal mol^{-1}).

TABLE I Chemical composition of the alloy (wt%)

Si	Mn	Fe	Cu	Mg	Zn	Ti	Al
0.6	1.0	0.7	0.15	0.20	0.10	0.20	Balance

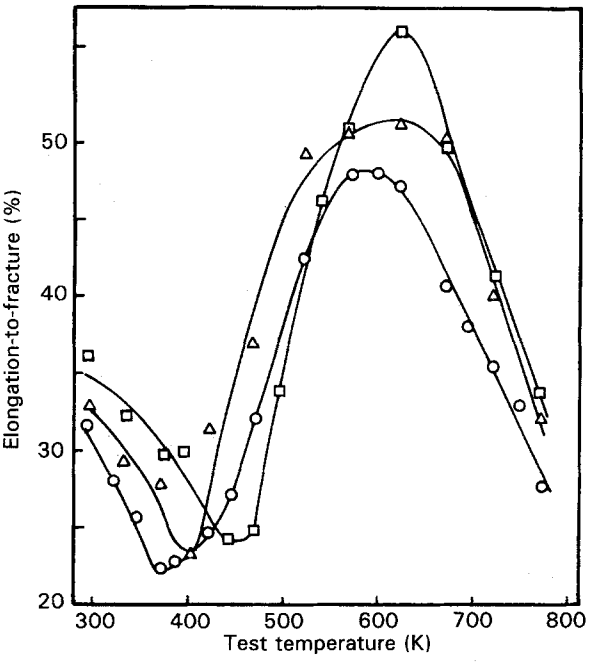

Figure 1 Effect of strain rate on the elongation-to-fracture versus the test temperature, for the following strain rates, $\dot{\varepsilon}$ (s^{-1}): (○) 5.56×10^{-5}, (△) 5.56×10^{-4}, and (□) 5.56×10^{-3}.

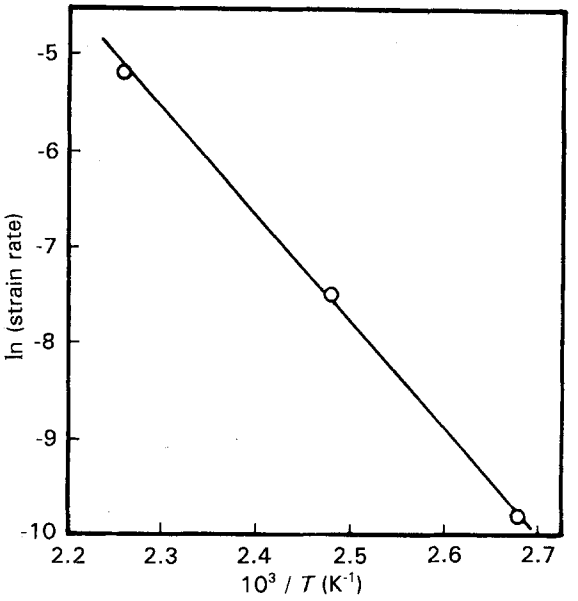

Figure 2 The linear relationship between the natural logarithm of strain rate and the reciprocal of the absolute temperature corresponding to the minimum in ductility.

The variation of 0.2% yield strength and UTS with test temperature is shown in Figs 3 and 4, respectively. In general, the behaviour in the following temperature ranges was: (a) 295–473 K (the range in which the material shows a loss of ductility), the yield strength increases while the UTS slightly decreased; (b) 473–623 K (the ductility increases up to maximum) both yield and UTS decreased rapidly; and (c) above 623 K, both yield and UTS slowly decreased while ductility drastically decreased.

Moreover, the strain rate affected the yield and UTS of the material. At lower temperatures (below 498 K),

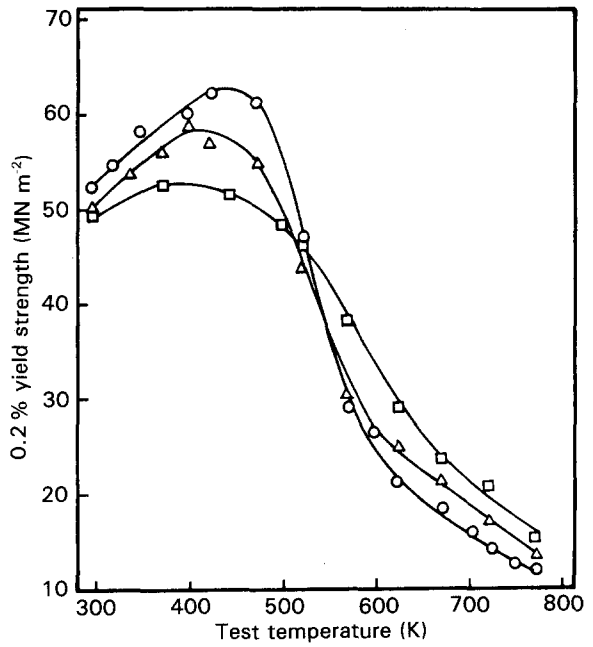

Figure 3 Effect of strain rate on 0.2% yield stress at various test temperatures, for the following strain rates, $\dot{\varepsilon}$ (s^{-1}): (○) 5.56×10^{-5}, (△) 5.56×10^{-4}, and (□) 5.56×10^{-3}.

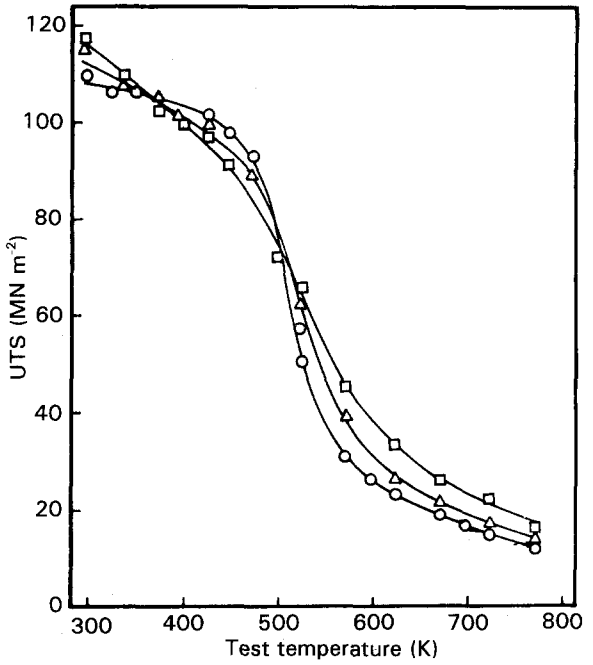

Figure 4 Effect of strain rate on the UTS at various test temperatures, for the following strain rates, $\dot{\varepsilon}$ (s^{-1}): (○) 5.56×10^{-5}, (△) 5.56×10^{-4}, and (□) 5.56×10^{-3}.

the yield and UTS varied inversely with strain rate while they were directly related above 498 K. In order to express this more clearly, an empirical relationship between the yield stress and the square root of the testing temperature at different strain rates can be written as [6, 12].

$$\sigma_T = \sigma_0 - mT^{1/2} \quad (1)$$

where, σ_T is the yield strength at test temperature T (K), σ_0 is the yield strength of the material at absolute zero, and m is the gradient of the straight line. The gradient, m, of the relationship is strain-rate dependent (Fig. 5).

In order to study the kinetics of the process responsible for the loss in yield strength of the alloy at elevated temperatures, the variable affecting the gradient, m, of Equation 1 should be removed, relating the strain rate to the temperature at a constant value of the yield strength. Fig. 5 gives the corresponding values of test temperatures at a constant yield strength of 18 MN m^{-2} for the applied strain rates. Fig. 6 plots the logarithm of the strain rate against the reciprocal of the testing temperature obtained from the intersections of the line of the constant yield stress with the straight lines obtained for the three different strain rates (Fig. 5). The relationship is linear, and it follows the Arrhenius rate equation yielding an activation energy of 258.5 kJ mol^{-1} (61.3 kCal mol^{-1}), Fig. 6.

Stress–strain curves have been used by a number of investigators, because of their sensitivity to material and test conditions and because a mathematical expression can be used to represent, analyse and compare them. Fig. 7 presents true-stress–true-strain curves for specimens tensile tested at a strain rate of $5.56 \times 10^{-4}\ s^{-1}$ in the temperature range 295–773 K. Fig. 8 presents the effect of the strain rate on the flow stress. The results indicate that, at constant strain, the flow stress decreases with increasing temperature but slightly decreases in the temperature range in which the material shows a loss in ductility. On the other hand, at constant temperature, the flow stress increases with increasing strain rate.

The general equation describing plastic deformation at both low and elevated temperatures [1, 3, 7, 16] is

$$\sigma = K_1 \varepsilon^n \dot{\varepsilon}^m \quad (2)$$

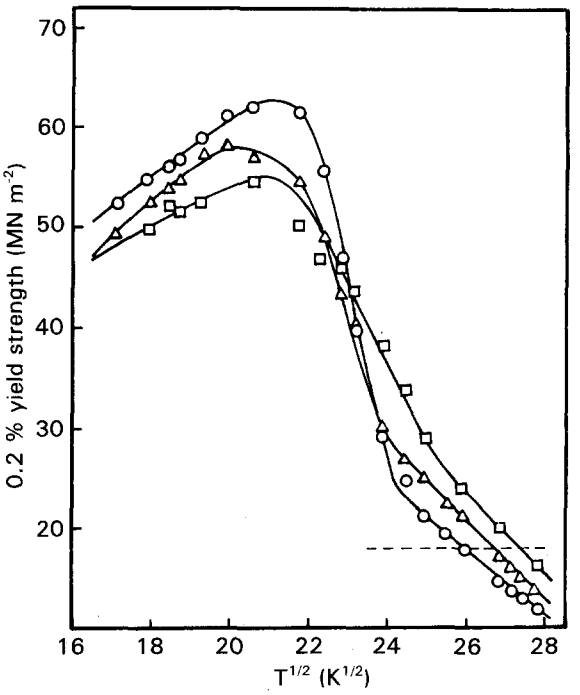

Figure 5 The relationship between yield strength and the square root of the test temperature, for the following strain rates, $\dot{\varepsilon}$ (s^{-1}): (○) 5.56×10^{-5}, (△) 5.56×10^{-4}, and (□) 5.56×10^{-3}.

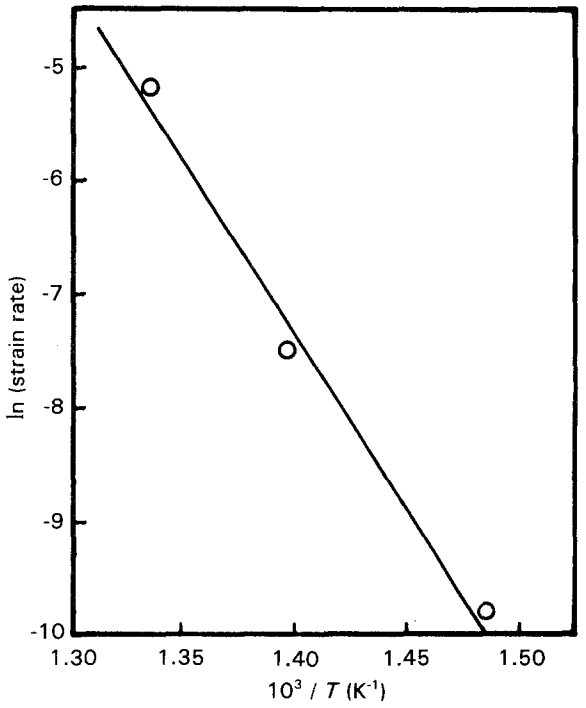

Figure 6 The linear relationship between the natural logarithm of the strain rate and the reciprocal test temperature corresponding to the constant yield strength 18 MN m^{-2}.

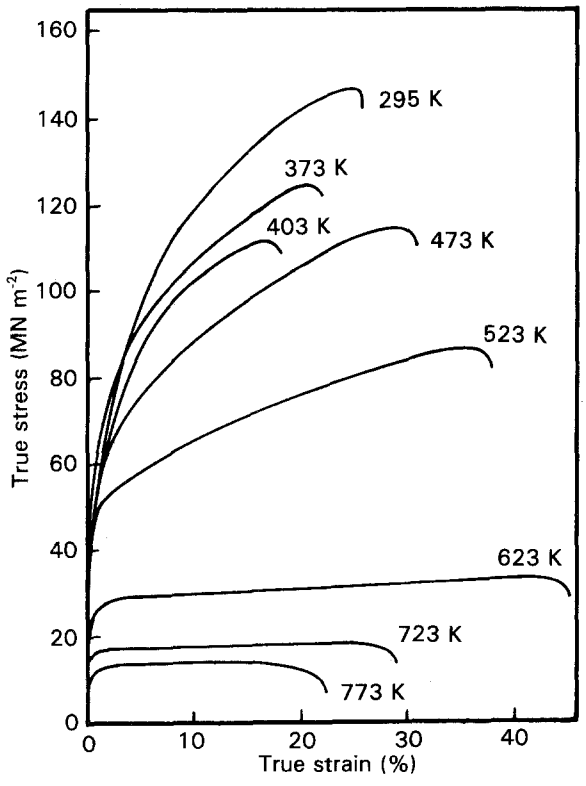

Figure 7 True-stress–true-strain relation as a function of temperature for specimens tested at a strain rate of 5.56×10^{-4} s^{-1}.

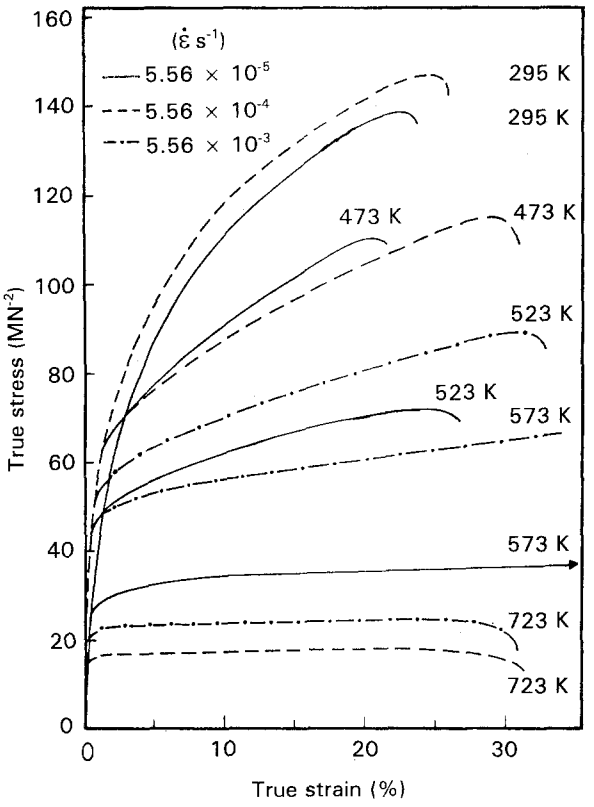

Figure 8 True-stress–true-strain relation as a function of temperature and the following strain rates: (—) 5.56×10^{-5}, (----) 5.56×10^{-4}, and (-·-·-) 5.56×10^{-3}.

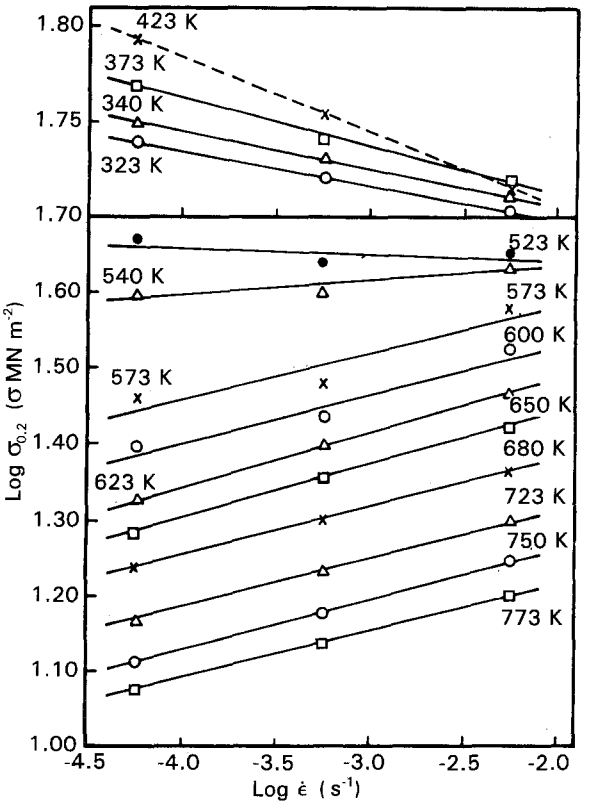

Figure 9 Log(0.2% yield stress) versus log(strain rate) relation as a function of the test temperature.

where, σ is the flow stress, ε the strain, $\dot{\varepsilon}$ the strain rate, n the strain-hardening index, m the strain-rate-sensitivity index and K_1 the material constant. At low temperatures this equation simplifies to

$$\sigma = K_2 \varepsilon^n \quad (3)$$

While at elevated temperatures it has the form

$$\sigma = K_3 \dot{\varepsilon}^m \quad (4)$$

Where K_2 and K_3 are also the material constants. From Equation 4, m was evaluated as the slope of the log $\sigma_{0.2}$ versus log $\dot{\varepsilon}$ plots as shown in Fig. 9. The

strain-rate sensitivity, m_1, is plotted against the test temperature in Fig. 10. The results indicate that there are two drops, as well as a minimum value, in the strain-rate sensitivity in the temperature range in which the material shows a loss in ductility as well as at minimum ductility (Fig. 1).

According to Ludwik [17] (Equation 3), every stress–strain curve which has a yield stress and a saturation stress becomes s-shaped, because the gradient, $d(\log \sigma)/d(\log \dot{\varepsilon})$ at low and high strains becomes zero. Around the inflection point, the curve can be approximated by a straight line, whose gradient gives the value of n [7–9, 12]. In the present work, n

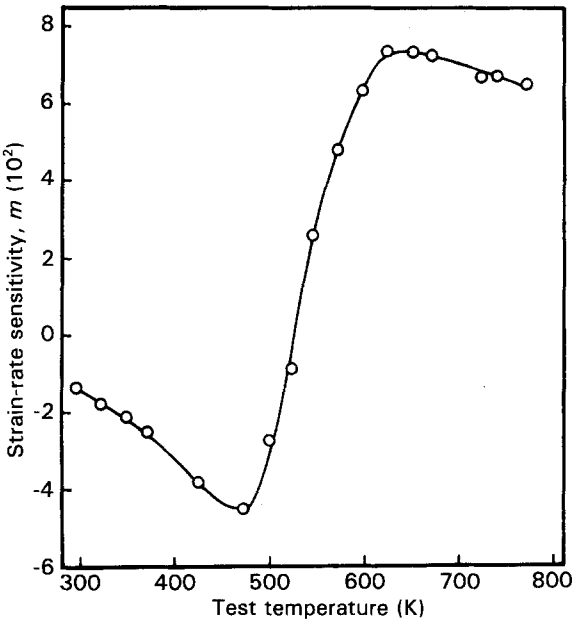

Figure 10 Strain-rate-sensitivity parameter, m, as a function of test temperature.

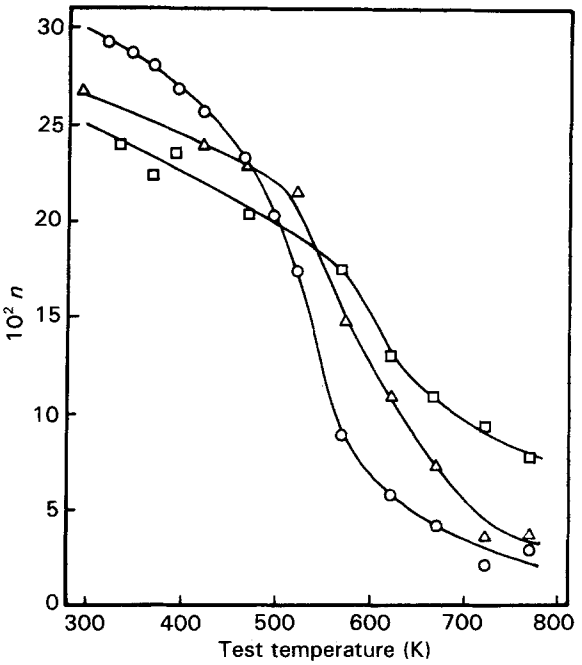

Figure 11 Effect of strain rate on the strain-hardening index, n at various temperatures, for the following strain rates, $\dot{\varepsilon}$ (s^{-1}): (○) 5.56×10^{-5}, (△) 5.56×10^{-4}, and (□) 5.56×10^{-3}.

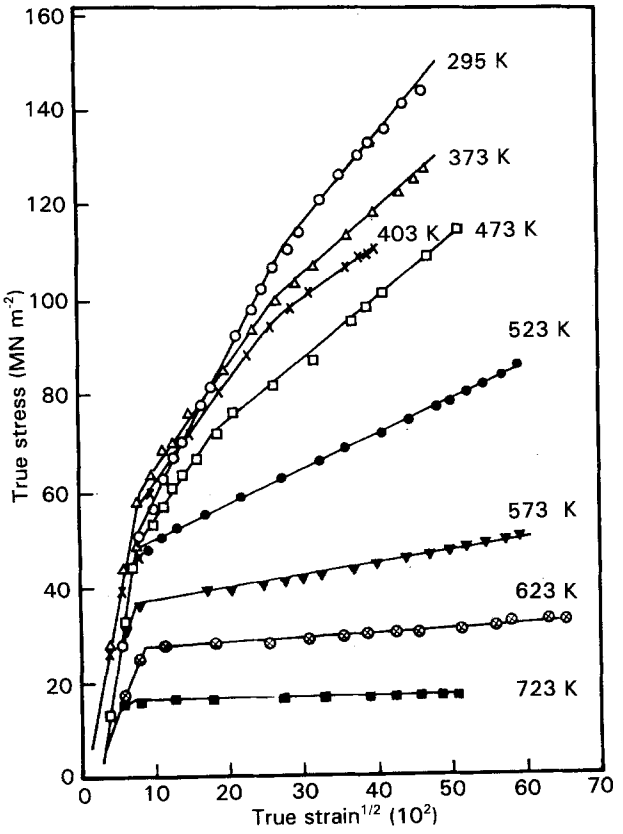

Figure 12 True-stress-(true strain)$^{1/2}$ relationship at various temperatures for a strain rate, $\dot{\varepsilon} = 5.56 \times 10^{-4}$.

was evaluated as the gradient of log(true stress) versus log(true strain), for specimens tensile tested at different temperatures and strain rates. The strain-hardening index, n, corresponding to the material tensile tested at the three strain rates is plotted against the test temperature in Fig. 11. The behaviour of the curves are very similar to those showing the effect of test temperature and strain rate on the UTS in Fig. 4.

Following earlier work [1, 3–9], the true stress and strain rates of specimens tensile tested at different temperatures are plotted against (true strain)$^{1/2}$ in Fig. 12 (for specimens tensile tested at a strain rate of $5.56 \times 10^{-4}\,s^{-1}$). The results indicate that in the temperature range 295–473 K there are three linear portions of different gradients and two linear parts above 473 K.

4. Discussion

The most important aspect of any engineering material is its structure, because its properties are closely related to this feature. Materials engineers must have a good understanding of this relationship between structure and a material's properties. From another point of view, the consistent achievement of a given strength requires the careful combination of a large number of both alloy and process variables, including the concentration of the major hardening elements, minor alloying additions and temperature. In general, any material for structural applications needs to have some ductility, so that it will accommodate local stresses by plastic deformation.

The results of the present work indicate that the

general behaviour of the change in ductility with temperature for specimens tensile tested at three strain rates is the same, i.e. there are two drops in ductility in the elongation-to-fracture versus temperature curves. The magnitude of these ductility drops as well as the temperature corresponding to minimum ductility decreases with decreasing strain rate. The yield strength increases with temperature up to the temperature corresponding to the minimum ductility. Thus, changes in properties observed in the tensile tests have to be understood in terms of precipitation which takes place in the starting material and that formed during the tensile tests at elevated temperatures. Since our transmission electron microscope is not working, the microstructural changes accompanying ageing and deformation will be interpreted according to our previous work.

The major impurities in the present material are Si, Mn and Fe. Addition of Si decreases the plasticity of Al. In the Al–Si system the equilibrium phases are Al and diamond cubic Si. Moreover, the solubility of Si in Al at 750 K is 0.7 wt% [18, 19]. Accordingly, the Si precipitate is stable in the corresponding temperature range between the first maximum and minimum in ductility (Fig. 1). On the other hand, the strain rate affected the magnitude of the drop in ductility as well as the temperature corresponding to the minimum. These results are in good agreement with previous work by the authors and co-workers [1, 6, 7, 10–13]. Moreover, the process responsible for the drop in ductility is both time and temperature dependent with an activation energy of 93.3 kJ mol^{-1} (22.1 kCal mol^{-1}, Fig. 2). This indicates that such a process is diffusion controlled. Compare the value obtained for the activation energy with that of diffusion of Si in Al, 82.0 kJ mol^{-1} (19.6 kCal mol^{-1}) [1, 20]. Further, in this temperature range, 295–473 K, Hammad *et al.* [1, 2] found Si precipitates in deformed commercial Al, and its size increased with temperature. Moreover, consistent with the observation of Harries and Varley [21] the precipitation of Si took place preferentially along the grain boundaries [2, 21]. Further, Petty [22] has noted that Si in Al alloys behaves in a brittle manner up to 625 K, while Ravi and Philofsky [23] have concluded that coarsening of the Si precipitates leads to a loss in ductility. Thus, with an increase in temperature, grain/sub-grain boundary mobility and dislocation motion are more severely impeded leading to the loss in ductility and the increase in yield strength [1, 2]. Accordingly, in view of the above, the decrease in ductility and the accompanying increase in yield strength with increasing temperature in the region of Si-precipitate stability is reasonable.

Above the temperature of minimum ductility and up to the second maximum in ductility (473–623 K), redissolution of Si is expected [1, 2]. On the other hand, since precipitation leads to a retardation of grain growth, it looks likely that thermal softening effects dominate in this range. Accordingly, a sudden increase in ductility, and a sharp decrease in the yield, the UTS and the strain-hardening index, n, was noticed above 573 K (Figs 1, 3, 4, 11).

Beyond the temperature of the second maximum in ductility (above $\sim$ 573 K), the ductility decreases while 0.2% yield stress, UTS, flow stress and strain-hardening index, n, slightly decrease with increasing temperature. Moreover, the maximum solubility of Fe and Mn at the eutectic temperatures 933 and 931 K are 0.052 and 1.25 wt%, respectively [18, 19]. Thus, some of the Fe and Mn should have precipitated as Al_3Fe [1, 2] and $MnAl_6$ [8, 9] even during solidification. Moreover, among the expected second-phase particles present in Al–0.95 wt% Si–0.5 wt% Mn and Al–0.99 wt% Si–0.21 wt% Mn is an α–$Al_{12}Mn_3Si$ phase [24]. The activation energy of 285.5 kJ mol^{-1} (61.3 kCal mol^{-1}) was obtained from the loss in yield strength as a function of test temperature for different strain rates (Fig. 5) and the corresponding plot of the logarithm of the strain rate versus the reciprocal of the absolute temperature (Fig. 6). The bulk diffusion of Fe in high purity aluminium, on the other hand, requires an activation energy of 260.8 kJ mol^{-1} (62.1 kCal mol^{-1}) [1, 25]. Accordingly, the process responsible for the loss in strength at high temperatures is diffusion controlled, i.e. the diffusion of Fe in Al to form Al_3Fe phase. Thus, from the above, the loss of ductility, yield and UTS, strain-hardening-exponent, n, above the temperature of the second maximum in ductility (above $\sim$ 623 K, Fig. 1), is due to the presence of precipitated particles of $MnAl_6$ [8, 9], $FeAl_3$ [1, 2] formed during ageing and deformation and the presence of an α–$Al_{12}Mn_3Si$ phase [24].

The observed drop in ductility due to precipitation should be accompanied by an increase in the yield stress [26]. In the present experiments the yield stress does increase with temperature up to a certain peak, in agreement with the above finding. Above this temperature ($\sim$ 473 K), the yield stress (Fig 3), UTS (Fig. 4), flow stress (Fig. 7) and hardening index, n, (Fig. 11) were decreased drastically due to thermal softening. Thus the actual value of the strength at any given temperature may be considered to be the resultant of these two opposing effects. Although precipitation should lead to an increase in the UTS, thermal softening appears to be slightly more dominant in this range.

As precipitation is a time-dependent process, for fixed experimental conditions an increase in the strain rate should be accompanied by a decrease in the severity of precipitation [3]. The inverse dependence of yield and UTS (Figs 3 and 4), flow stress (Fig. 8) and strain-hardening index, n, (Fig. 11), on the strain rate in the temperature range 295–523 K, is due to the decrease in the severity of precipitation with increasing strain rate. The negative or nearly zero gradients, m, of the log σ versus log $\dot{\varepsilon}$ plots (Fig. 9) in this range indicates that the flow could be represented by Equation 3. The direct relation between the 0.2% yield and the strain rate above 523 K, however, indicates that in this temperature range (n is practically zero, Fig. 11) the effect of precipitation is not so important since the conventional dependence of stress on strain rate and Equation 4 govern the flow.

Moreover, the value of the strain-rate sensitivity, m, does not increase monotonically with temperature

(Fig. 10) as in the case for a simple thermally activated process [1, 3, 7]. There is a minimum at 473 K which is consistent with the same temperature range in which the material shows a loss in ductivity. Furthermore, over the whole temperature range, the temperature dependence of the strain-rate sensitivity, m, follows the same trend as that of the elongation (Figs 1 and 10). Therefore, the elongation minimum can also be explained in terms of the strain-rate-sensitivity minimum [27]. When a neck forms, the strain in the necked region increases. If the strain-rate-sensitivity is high, the increase of strain rate in the necked region may sufficiently increase the resistance to flow for deformation to occur above and below the neck. On the other hand, the low value of the strain-rate sensitivity concentrates the deformation in the neck, once a neck is formed, resulting in low ductility. Moreover, the present results were similar to those obtained by Lee [28], Hong *et al.* [27] for zircaloy-4 and Hammad *et al.* [12] for Zr–1% Nb alloy.

Following earlier work [1, 3–9], the true stress of specimens tensile tested at different strain rates and temperatures were plotted against (true strain)$^{1/2}$ (Fig. 12, for tests at a strain rate of $5.56 \times 10^{-4}\ s^{-1}$). The results indicate that, up to 473 K there was a need to divide the range into three linear portions of different gradients, but, as previously [1, 3–9] into only two linear parts above 473 K. The appearance of the third portion in the present study may be due to the presence of Si, Mn and Fe.

5. Conclusions

The elevated-temperature tensile properties of solution-treated Al–0.6% Si–1% Mn–0.7% Fe alloy, tensile tested at different strain rates, led to the following conclusions.

1. Two troughs in the elongation-to-fracture versus the temperature-of-deformation curves were encountered due to the precipitation of Si, Al_3Fe, $MnAl_6$ and α–$Al_{12}Mn_3Si$.

2. Strain rates affect the magnitude of the drop in ductility as well as the temperature corresponding to the minimum ductility. The slower the strain rate the greater is the magnitude of the drop in ductility and the lower is the temperature corresponding to the minimum value of the elongation-to-fracture.

3. Activation-energy measurements revealed that diffusion of Si along dislocation and/or grain boundaries and the diffusion of Fe in either Al_3Fe or in the present alloy, were the rate-controlling steps in the vicinity of the first and the second drop in ductility, respectively.

4. The elevated temperature 0.2% yield and UTS, strain-hardening exponent and strain-rate sensitivity were found to be strain-rate dependent and could be explained on the basis of the precipitation processes.

5. At low and high temperatures the flow could be represented by the equations $\sigma = K_2 \varepsilon^n$, $\sigma = K_3 \dot{\varepsilon}^m$, respectively.

6. There is a minimum in the strain-rate sensitivity versus temperature curve in the temperature range which is coincident with the elongation-minimum temperature range, and over the whole temperature range the temperature dependence of the strain-rate sensitivity follows the same trend as that of the elongation-to-fracture.

7. The σ versus $\varepsilon^{1/2}$ plots indicate that up to 473 K there was a need to divide the range into three linear portions of different gradients but into only two linear portions above 473 K.

References

1. A. M. HAMMAD, K. A. PADMANABHAN and T. R. ANANTHARAMAN, *Trans. Ind. Inst. Metals* **30** (1977) 327.
2. A. M. HAMMAD, K. A. PADMANABHAN, G. V. TENDELOO and T. R. ANANTHARAMAN, *Trans. Ind. Inst. Metals*, **30** (1977) 338.
3. A. M. HAMMAD, K. A. PADMANABHAN, G. V. TENDELOO and T. R. ANANTHARAMAN, *Z. Metallkde* **78** (1987) 103.
4. A. M. HAMMAD, K. A. PADMANABHAN, G. V. TENDELOO and T. R. ANANTHARAMAN, *Z. Metallkde* **78** (1987) 113.
5. A. M. HAMMAD, K. K. RAMADAN and M. A. NASR, *Z. Metallkde* **80** (1989) 173.
6. A. M. HAMMAD and K. K. RAMADAN, *Z. Metallkde* **80** (1989) 178.
7. A. M. HAMMAD and K. K. RAMADAN, *Z. Metallkde* **80** (1989) 431.
8. A. M. HAMMAD and O. A. RUGBANI, *High Temp. Technol.* **8** (1990) 261.
9. A. M. HAMMAD, M. A. SHABAN and S. M. SHERIF, *J. Mater. Sci.* **26** (1991) 6331.
10. A. M. HAMMAD, *Trans. Ind. Inst. Metals* **40** (1987) 39.
11. A. M. HAMMAD, *Trans. Ind. Inst. Metals* **40** (1987) 423.
12. A. M. HAMMAD, S. M. EL-MASHRI and M. A. NASR, *J. Nucl. Mater.* **186** (1992) 166.
13. I. A. EL-SHANSHOURY, F. I. GADALLAH and A. M. HAMMAD, *J. Nucl. Mater.* **42** (1972) 203.
14. I. A. EL-SHANSHOURY and F. I. GADALLAH, *J. Nucl. Mater.* **36** (1970) 87.
15. I. A. EL SHANSHOURY, I. A. VORONIN and M. S. ABDELAZIM, *J. Nucl. Mater.* **29** (1969) 161.
16. G. J. DAVIES, J. W. EDINGTON, C. P. CULTER and K. A. PADMANABHAN, *J. Mater. Sci.* **5** (1970) 1091.
17. P. LUDWIK, "Elemente der technologischen mechanik", (Springer, Berlin, 1960).
18. L. F. MONDOLFO, "Aluminium alloys, structure and properties", (Butterworths, London, 1976) pp. 229, 284.
19. R. P. ELLIOTT, "Constitution of Binary Alloys", First Supplement, (McGraw-Hill, New York, 1965) p. 55.
20. G. J. VANGURP, *J. Appl. Phys.* **44** (1973) 2040; see also *Diffusion Data* **7** (1973) 527.
21. I. A. HARRIES and P. C. VARELY, *J. Inst. Metals* **82** (1953–54) 379.
22. E. R. PETTY, *J. Inst. Metals* **91** (1962–63) 274.
23. K. V. RAVI and E. PHILOFSKY, *Met. Trans.* **2** (1971) 711.
24. D. M. R. TAPLIN, The Physical Metallurgy of Fracture, Fourth International Conference on Fracture (University of Waterloo, Canada) 2A (1977).
25. G. M. HOOD, *Phil. Mag.* **21** (1970) 305.
26. J. W. MARTIN, "Precipitation hardening", (Pergamon, Oxford, 1968) p. 29.
27. S. I. HONG, W. S. RYU and C. S. RIM, *J. Nucl. Mater.* **116** (1983) 314.
28. D. LEE, *Can. Metall. Quart.* **11** (1972) 1321.

Received 8 May 1992
and accepted 3 February 1993